10th ANKARA INTERNATIONAL AEROSPACE CONFERENCE **AIAC-2019-040**
18-20 September 2019 - METU, Ankara TURKEY

ATOMIZATION AND COMBUSTION CHARACTERISTICS OF IMPINGING INJECTORS IN LIQUID ROCKET ENGINES

Burak Cenik[1] and Tacettin Utku Suer[2]
TOBB University of Economics and Technology
Ankara, Turkey

Sitki Uslu[3]
TOBB University of Economics and Technology
Ankara, Turkey

ABSTRACT

Computational fluid dynamics (CFD) simulations of a like-on-like jet impingement injector that experimentally and analytically studied at Pennsylvania State University are performed in this paper. Large Eddy Simulations of the like-on-like injector are accomplished and break-up length and drop size distribution are compared with validation data measured with a phase Doppler particle analyzer (PDPA). CFD simulations of an unlike triplet injector are performed under cold-flow conditions with STAR CCM+ to investigate and compare the primary break-up characteristics of two types of injectors. For triplet injector, effects of different inlet velocity values on droplet size distributions, sheet formation and break-up length are investigated. In this study, it is observed that increasing the relative velocity between air and water, peaks of log-normal distributions are decreased.

INTRODUCTION

The Impinging injectors are based on the atomization process which is a result of the collision of two or more high speed jets. Impinging injectors can be designed in different types such as unlike doublet, triplet and pentad [Arienti, 2013]. A schematic diagram of a like-on-like injector is shown in Figure 1. The angle between jets is 2θ and it is typically 60 degree [Ryan, 1995]. The impinging injectors are generally used in liquid fuel engines. The injectors play an important role in combustion performance and stability by enhancing atomization and achieving a better mixing. Design processes must be performed carefully. Hence, cold flow experiments of primary atomization characteristics are substantial. Today, performing these experiments is still difficult and demanding due to the complexity of the process and the inability to measure near the injectors because of the limited optical access. Therefore, numerical analysis plays an essential role in the design process [Inoue 2009].

The main focus of this paper is to perform high fidelity simulations of an unlike triplet injector of a rocket engine and investigate their effects on combustion phenomenon. Firstly, CFD simulations of the like-on-like injector that studied at Pennsylvania State University, [Anderson, 1995; Ryan, 1995], are performed for validation purposes. The commercial CFD code Star CCM+ has been used for the computations. Secondly, an unlike triplet injector is

[1] M.Sc. Student in Department of Mechanical Engineering, Email: bcenik@etu.edu.tr
[2] M.Sc. Student in Department of Mechanical, Email: tusuer@etu.edu.tr
[3] Asst. Prof. in Department of Mechanical Engineering, Email: suslu@etu.edu.tr

going to be studied. Finally, the effects of impinging injector types on atomization characteristics and how the changes in atomization characteristics affects the combustion phenomenon are going to be examine.

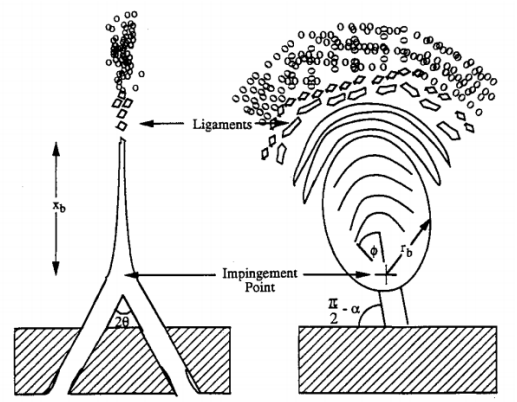

Figure 1: Schematic diagram of a typical impinging jet spray [Ryan, 1995]

METHOD

Numerical Method

In this study, three-dimensional large eddy simulations of a like-on-like impinging injector is performed with Wall-Adapting Local-Eddy Viscosity subgrid scale model (WALE). The Volume Of Fluid (VOF) method is used as a multiphase model to resolve the interface between the phases of the mixture. It is used to solve problems in CFD such as immiscible fluid mixtures, free surfaces, and phase contact time. It is based on the Eulerian approach of multiphase flow. The solver uses a 2nd order discretization scheme named as High Resolution Interface Capturing (HRIC) in order to obtain sharp interfaces between phases. The distribution of phases and the position of the interface are described by the fields of phase volume fraction α_i. The volume fraction of phase i is defined as [Siemens, 2019]:

$$\alpha_i = \frac{V_i}{V} \qquad \text{Equation (1)}$$

where V_i is the volume of phase i in the cell and V is the volume of the cell. The volume fractions of all phases in a cell must sum up to one:

$$\sum_{i=1}^{N} \alpha_i = 1 \qquad \text{Equation (2)}$$

where N is the total number of phases.
Depending on the value of the volume fraction, the presence of different phases or fluids in a cell can be distinguished:

- $\alpha_i = 0$, the cell is completely void of phase i
- $\alpha_i = 1$, the cell is completely filled with phase i
- $0 < \alpha_i < 1$, values between the two limits indicate the presence of an interface between phases

The material properties that are calculated in the cells containing the interface depend on the material properties of the constituent fluids. The fluids that are present in the same interface-containing cell are treated as a mixture:

$$\rho = \sum_i \rho_i \alpha_i \quad \text{Equation (3)}$$

$$\mu = \sum_i \mu_i \alpha_i \quad \text{Equation (4)}$$

$$c_p = \sum_i \frac{(c_p)_i \rho_i \alpha_i}{\rho} \quad \text{Equation (5)}$$

Where ρ_i, μ_i and $(c_p)_i$ are the density, dynamic viscosity, and specific heat of phase i respectively.

Volume Fraction Transport Equation

The distribution of phase i is driven by the phase mass conservation equation:

$$\frac{\partial}{\partial_t}\int_V \alpha_i dV + \int_A \alpha_i \mathrm{v} \cdot d\mathrm{a} = \int_V (\mathrm{S}_{\alpha_i} - \frac{\alpha_i}{\rho_i}\frac{D\rho_i}{Dt})\,\mathrm{dV} - \int_V \frac{1}{\rho_i}\nabla\cdot(\alpha_i \rho_i \mathrm{v}_{d,i})\,\mathrm{dV} \quad \text{Equation (6)}$$

where a is the surface area vector, v is the mixture (mass-averaged) velocity, $\mathrm{v}_{d,i}$ is the diffusion velocity, S_{α_i} is a user-defined source term of phase i, and ρ_i / Dt is the material or Lagrangian derivative of the phase densities ρ_i.

STAR-CCM+ calculates the volume fractions of phases as follows:

- When there are two VOF phases present, the volume fraction transport is solved for the first phase only. In each cell, the volume fraction of the second phase is adjusted so that the sum of the volume fractions of the two phases is equal to 1.
- When there are three or more VOF phases present, the volume fraction transport is solved for all phases. The volume fraction of each phase is then normalized based on the sum of the volume fractions of all phases in each cell [Siemens, 2019].

If a non-zero sharpening factor is specified, an additional term is added to the VOF transport equation:

$$\nabla\cdot(\mathrm{v}_{ci}\,\alpha_i(1-\alpha_i)) \quad \text{Equation (7)}$$

where:

- α_i is the volume fraction of phase i
- v_{ci} is defined as follows:

$$\mathrm{v}_{ci} = C_\alpha \times |\mathrm{v}| \frac{\nabla\alpha_i}{|\nabla\alpha_i|} \quad \text{Equation (8)}$$

- C_α is the sharpening factor
- v is the fluid velocity

Validation and Mesh Independence Study

The experiments are accomplished under the different angle and velocity values. In this study, the angle and velocity of jets are 60 degree and 18.5m/s respectively. The liquid that is used in the experiment was water (ρ_l=0998 kg/m3, surface tension=0.076 N/m, and dynamic viscosity μ_l=0.0010 Pa.s). The computational domain size is 16 by 12 by 25 mm and droplets are sampled at a plane 20mm (Figure 2). The smallest grid size is 31.25 μm and uniform size cells are used in the liquid sheet region. Fixed time step (0.5 μs) was used and droplet data were sampled at 5.25 – 8.25 ms to avoid initial startup effects.

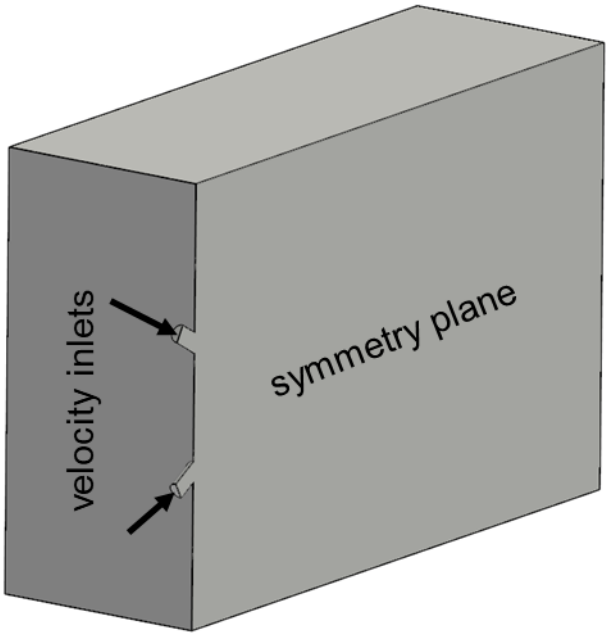

Figure 2: Computational domain

For validation case, firstly uniform cell size mesh is used and then adaptive mesh refinement (AMR) method is applied. For uniform cell size, smallest grid size defined as 31.25 μm and the smallest cells are concentrated at the liquid sheet area and uniform sized mesh is shown in Figure 3.

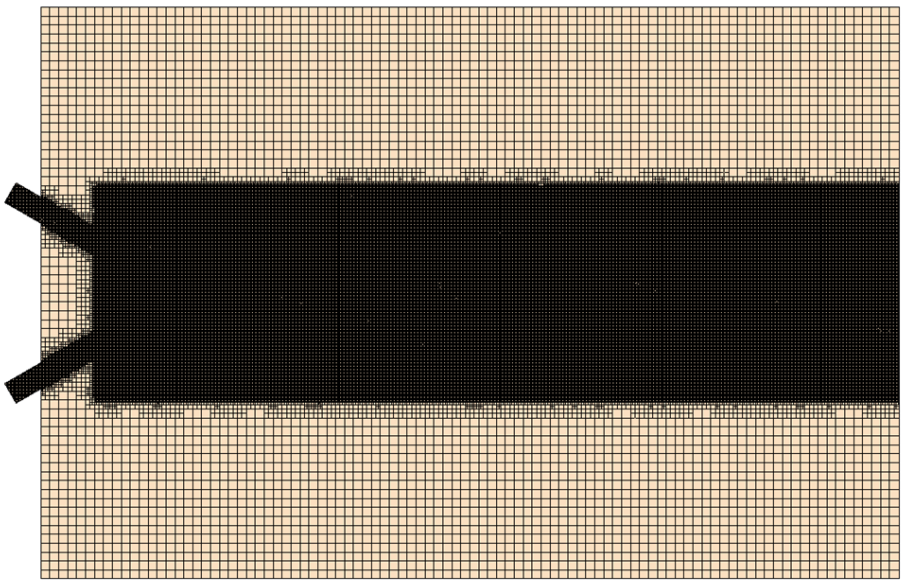

Figure 3. Uniform sized mesh scene for the like-on-like jet injector computational domain

Adaptive mesh refinement method is applied by using volume fraction gradient. Volume fraction gradient values are limited between 0 and 1 using Sigmoid Function that is given by Equation (9) as,

$$S(x) = \frac{1}{1+e^{-x}} \qquad \text{Equation (9)}$$

The smallest grid sizes are defined as 62.50 μm, 31.25 μm and 15.625 μm for the coarse, medium and fine level mesh size respectively. Total number of mesh values are given in Table 1.

Table 1. Mesh Study for the AMR

	The smallest grid size (μm)	Number of elements
Uniform Mesh	31.25	36 M
Coarse Mesh	62.50	200 K
Medium Mesh	31.25	1.4 M
Fine Mesh	15.625	8.1 M

The values given in the table 1 are the average values taken for the adaptive mesh study when the number of cells of the analyzes no longer changes much. The alteration in the total number of elements over time is given in Figure 4.

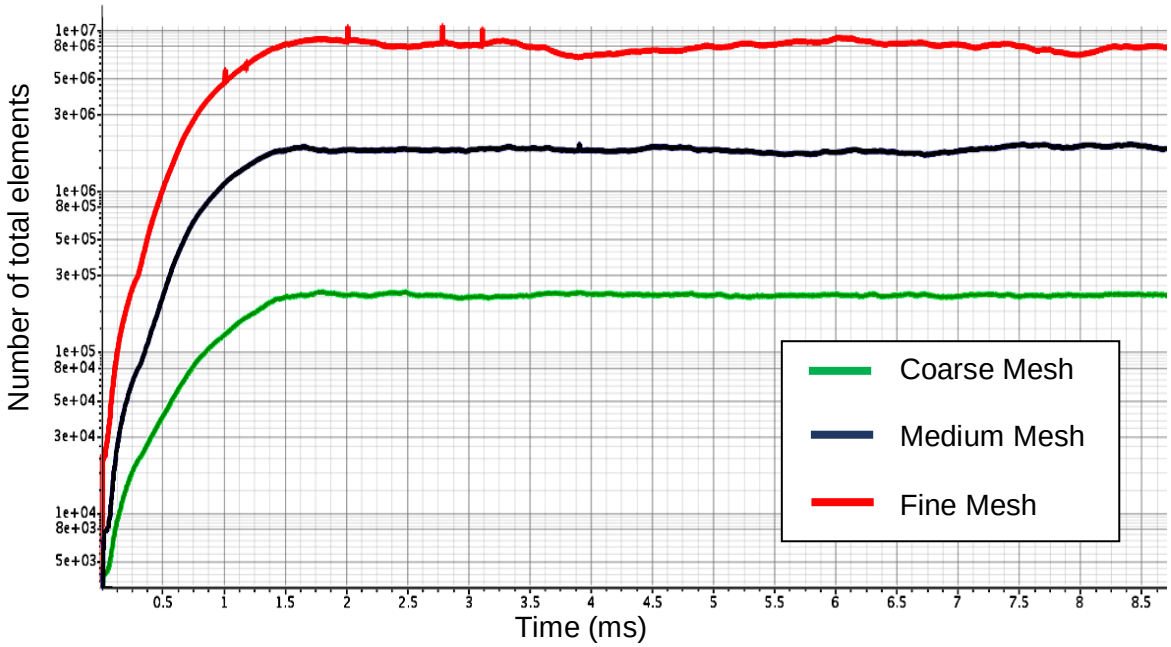

Figure 4. The alterations in the total number of elements over time

Coarse, medium and fine mesh contours are shown in Figure 5. Cells become smaller or larger with the change in volume fraction gradient. If the change is too high (close to 1), the cells concentrates there but if the change closes to 0, the cells get larger up to 1mm. How the flow behaves only by looking at the cells can be seen in Figure 5.

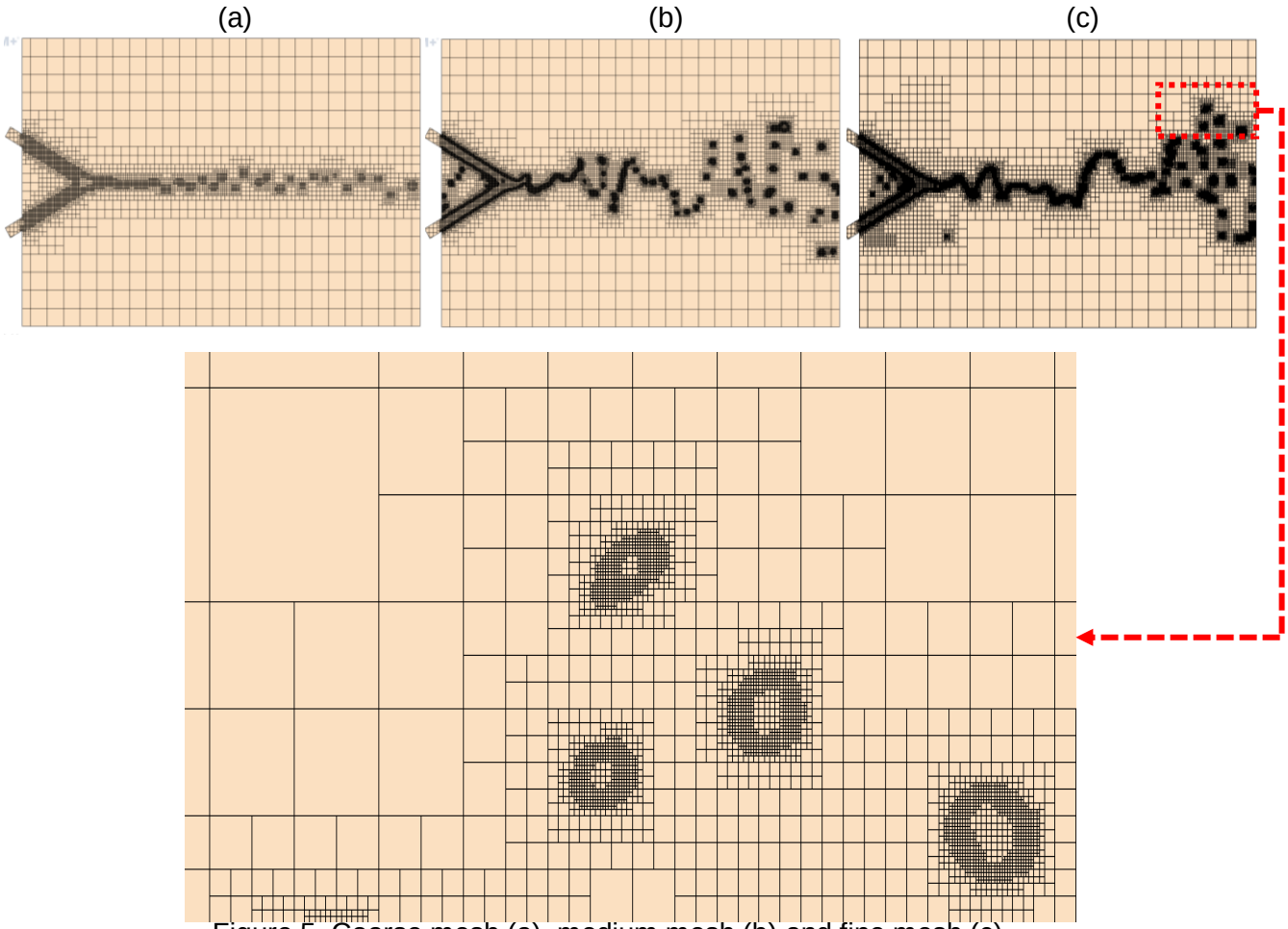

Figure 5. Coarse mesh (a), medium mesh (b) and fine mesh (c)

CFD results of like-on-like impinging injectors are compared with PDPA results that are performed before by Anderson et al. [Anderson, 1995]. In Figure 6, CFD results have a good agreement with PDPA data in droplet distribution. The difference between results of medium mesh and fine mesh can be tolerable considering CPU cost.

On the other hand, medium mesh and uniform-sized mesh have almost the same distribution and the comparison is given in Figure 7. From this results, AMR medium mesh is the most reasonable choice considering the CPU cost. For this reason, medium size adaptive mesh is used for the triplet injector numerical simulations.

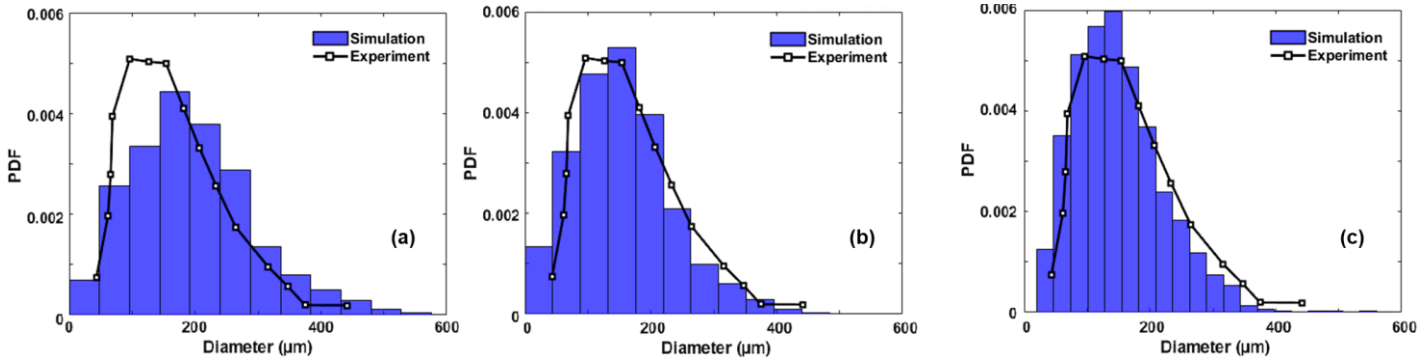

Figure 6. The Comparison of 3 levels of adaptive mesh (a-coarse, b-medium, c-fine mesh)

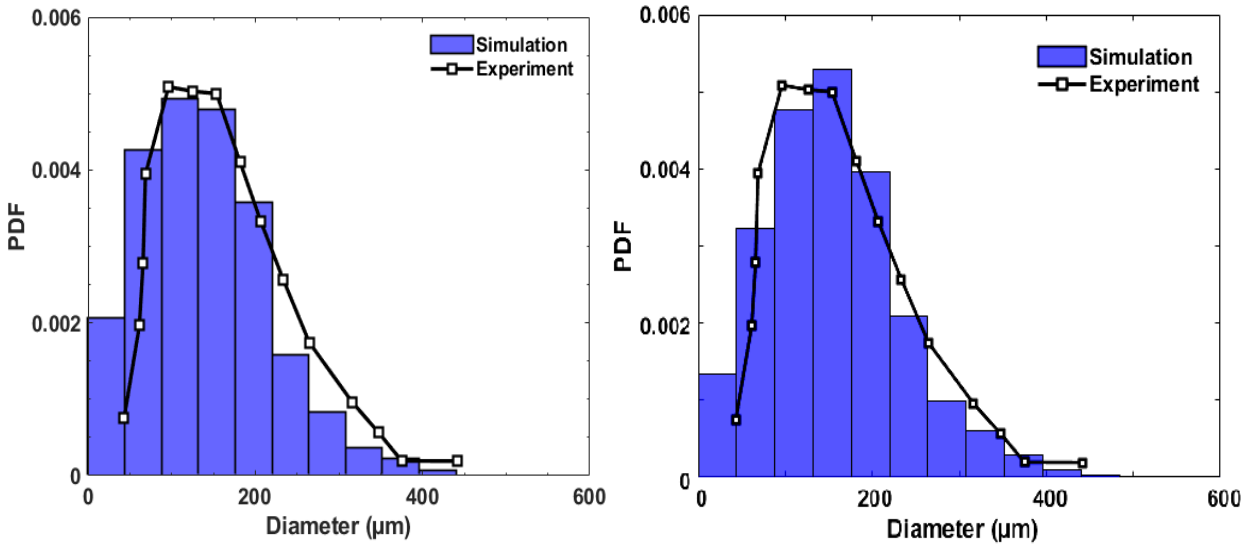

Figure7. Droplet size distibution of uniform-sized (left) and Adaptive-sized mesh (right)

Side view of snapshots of both simulation and experiment are shown in Figure 8. The sheet breakup length was measured to be 17.5 mm in experiment compared to a value of 10 mm predicted by CFD LES computations for uniform sized mesh. The sheet breakup length is estimated more accurately with a finer grid size. It is estimated maximum 16.5 mm and minimum 13.5 mm from the results of fine mesh.

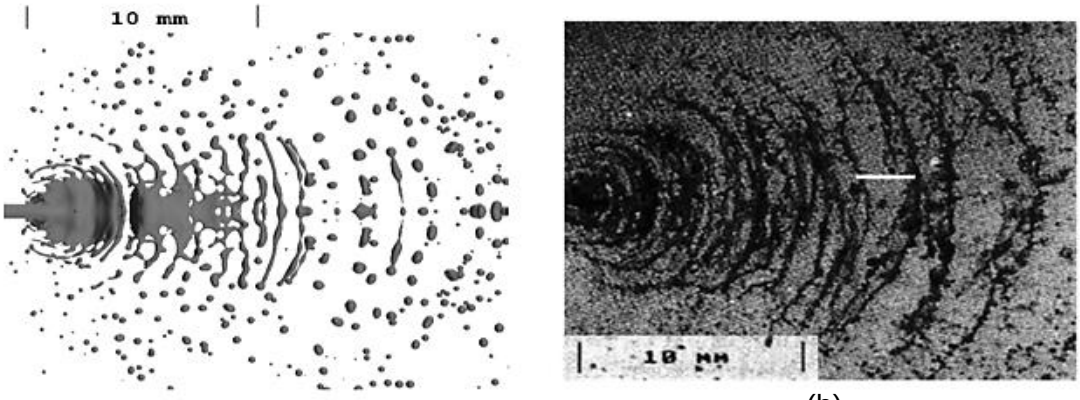

(a) (b)

Figure 8. Side view snapshot of the simulation is shown with (a), Snapshot of the experiment is shown with (b).

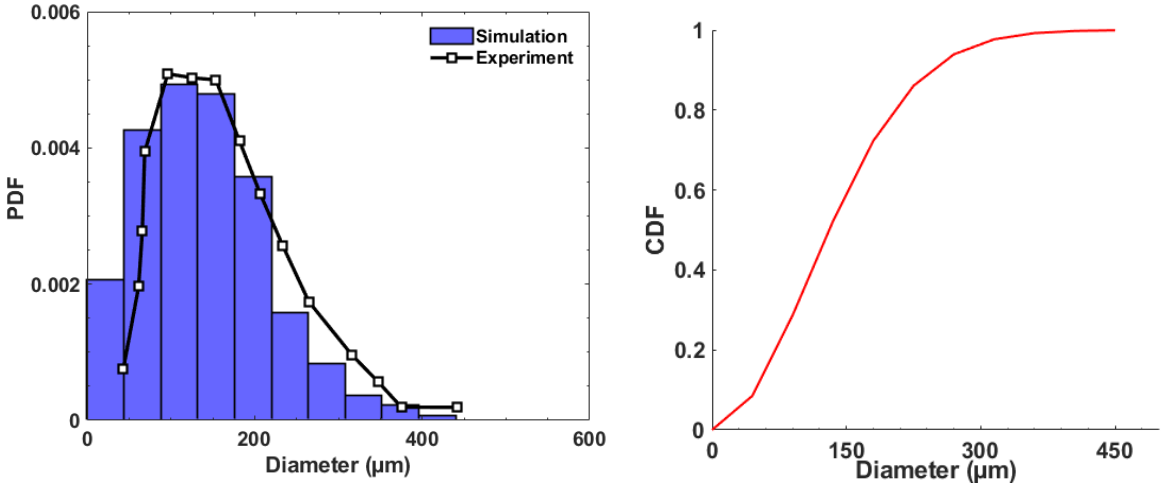

Figure 9: Comparison of the density distribution of droplet size of the experiment and the CFD LES simulation (left) and Cumulative Density Function of the Computation (right).

In Figure 9 droplet diameter peaks around 100 μm and CDF plot shows that 50% of the number of particles is at or below 132 μm.

Volume fraction contours in Figure 10 shows that coarse mesh could not give a fine resolution for the interface between air and water and mesh is getting finer, resolution capturing ability improves. It is observed from this side view that the sheet break-up length increases with finer mesh.

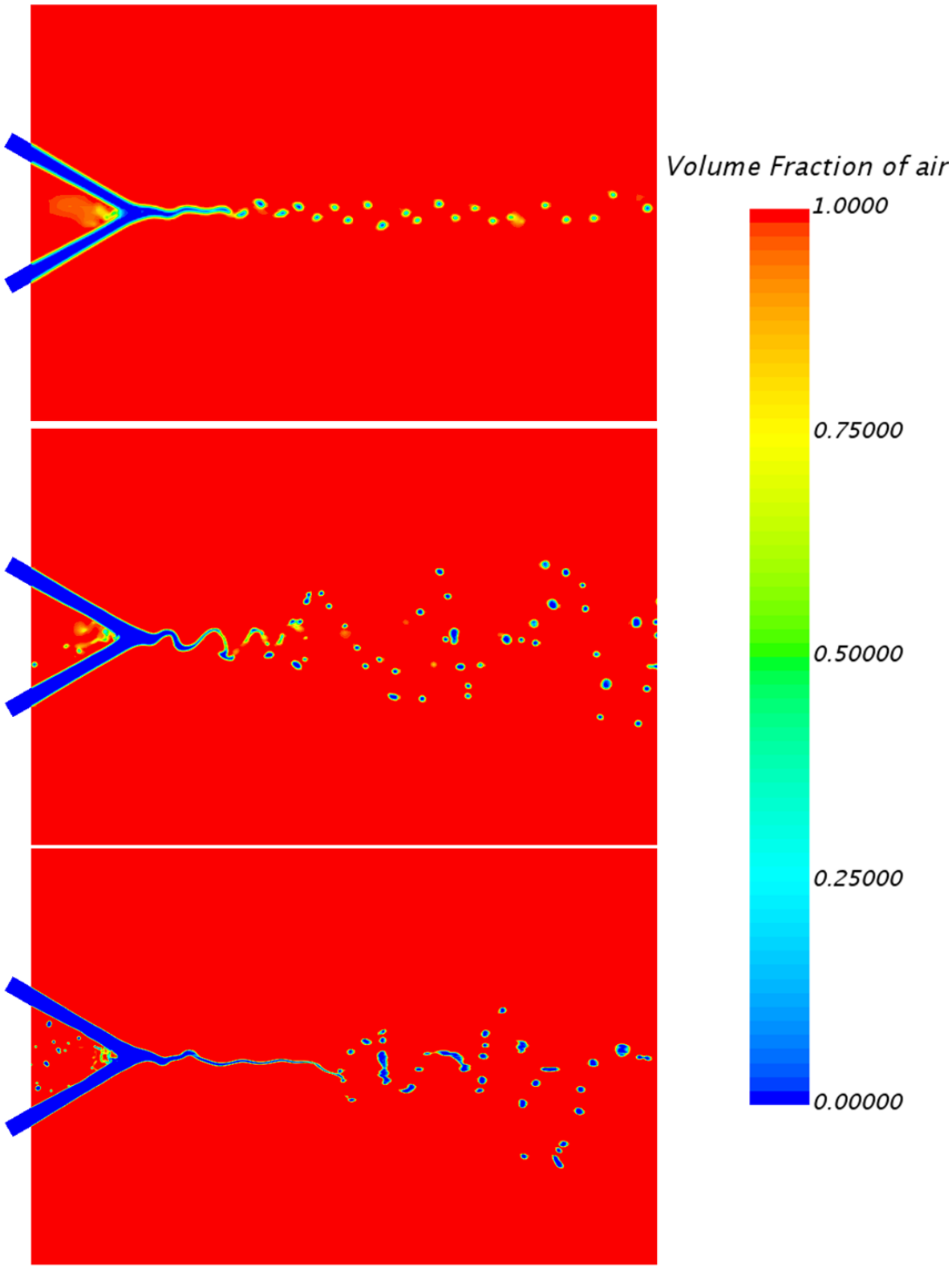

Figure 10. Volume fraction resutls of coarse (top), medium (middle), and fine (bottom) mesh

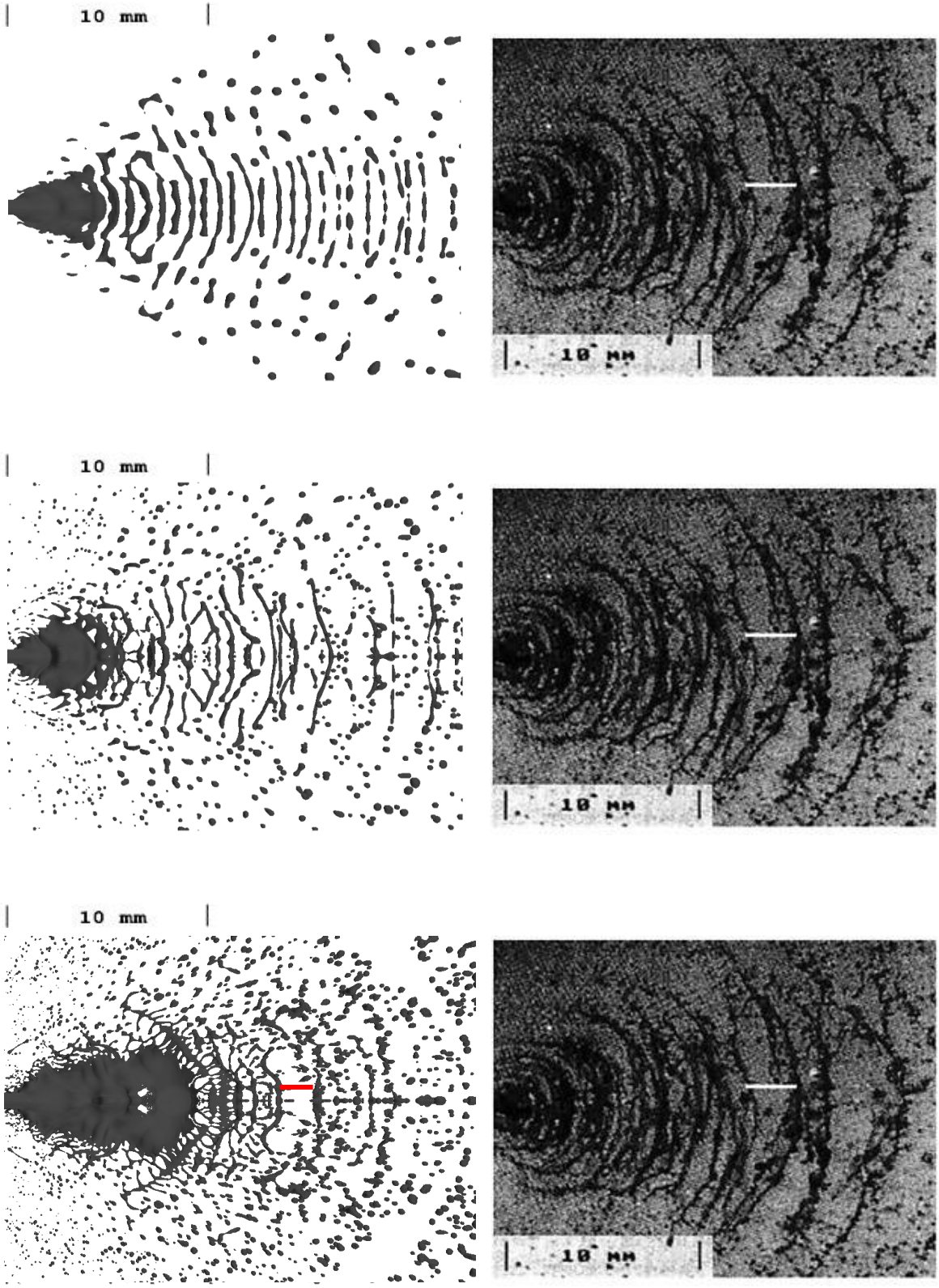

Figure 11. Sheet break-up length comparison with the experiment; coarse mesh (top), medium mesh (middle), fine mesh (bottom)

Liquid sheet is showed in Figure 11 and the same result can be seen that the break-up length increases and gets closer to the experiment with the finer mesh. In the coarse mesh, the liquid sheet disintegrated before medium and fine mesh. In addition, the particle sizes in

the computational domain generally are larger and small particles around the impingement point could not be observed. More detail of liquid sheet formation and primary break-up phonemena can be seen from Figure 12. The liquid sheet moves only impingement axial and has a monotonous formation in the coarse mesh while there are many fluctuations in the medium and fine mesh.

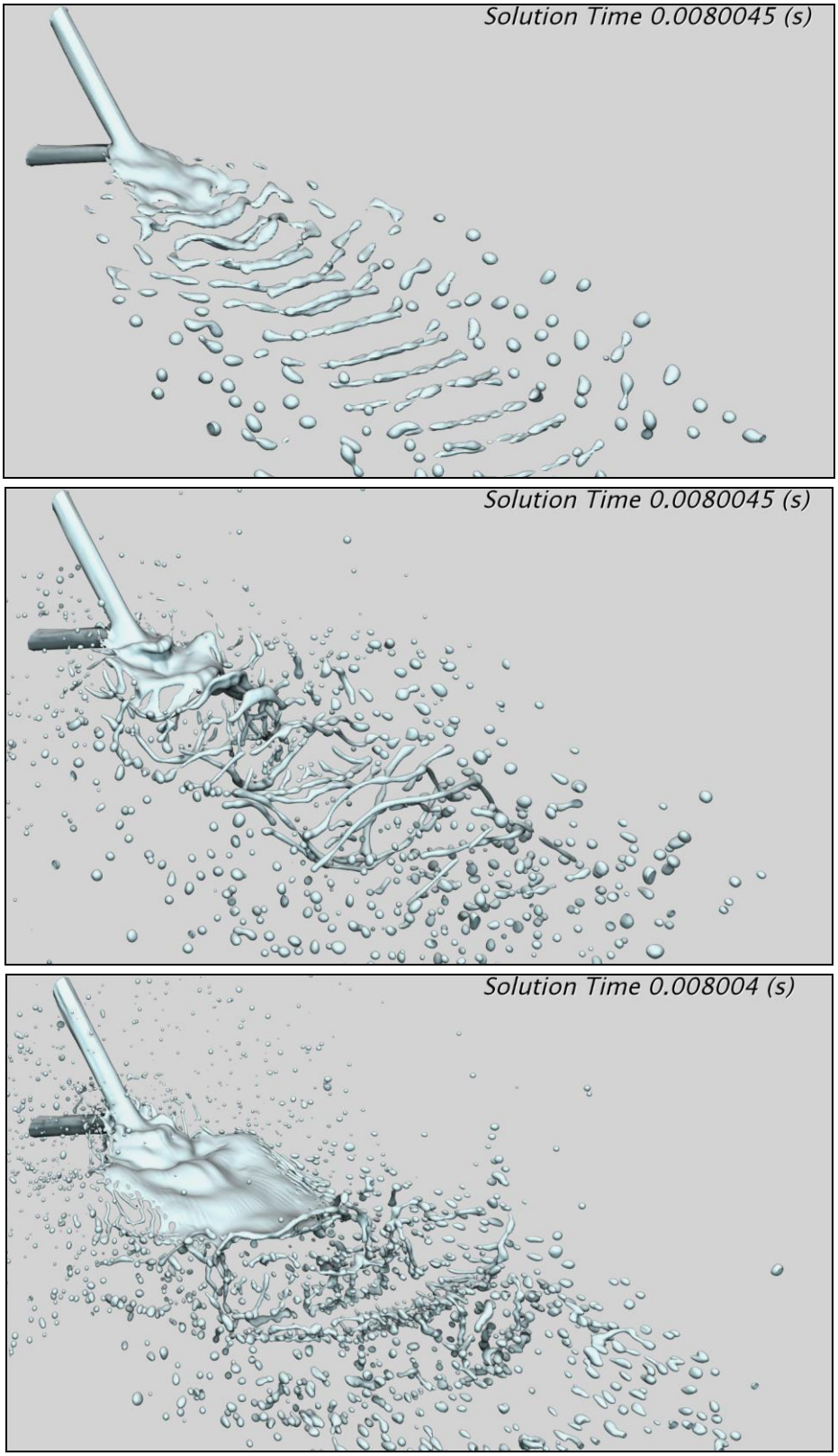

Figure 12. Coarse (top), medium (middle) and fine (bottom) mesh sheet formations and break-up characteristics

RESULTS AND DISCUSSIONS

After the like-on-like doublet impingement jet injector numerical analyses are completed, triplet impingement jet injector analyses are performed with the same procedure. In triplet injectors, generally two types of fluid are used; one of them is fuel and the other is oxidizer. In this study, only the water is used to simplify the problem. AMR technique is also applied for this case and medium mesh that has 31.25 μm smallest grid size is used.

Doublet and triplet impingement jet injector liquid sheets are shown in Figure 13. Triplet injector has more monotonous structure and sheet break-up length is approximately 2 times the doublet injector.

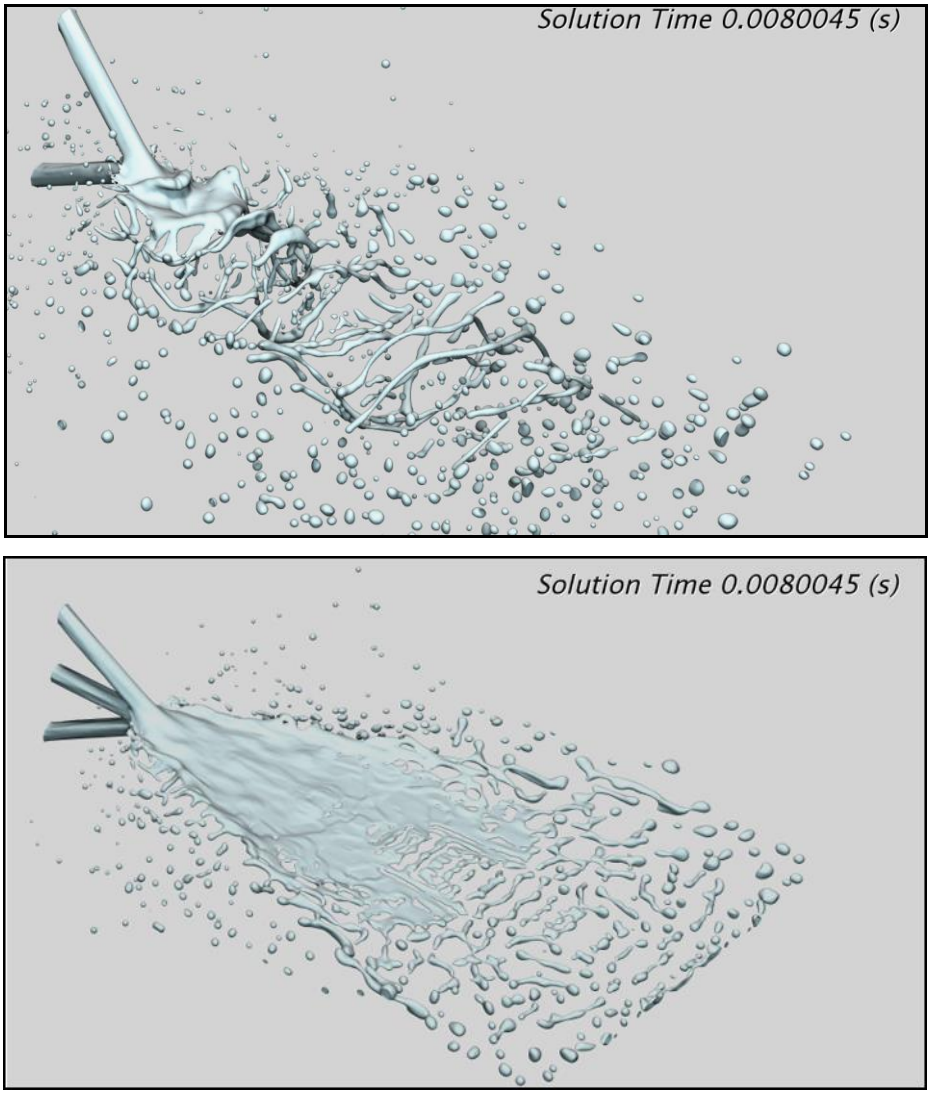

Figure 13. Liquid sheet formation and break-up process of doublet and triplet injectors

From the opposing point of view, droplet size distribution of two types of injectors is almost the same and it can be seen from Figure 14. In this study, third injector at the center affects the sheet length but the size distribution. In addition, liquid sheet occurs around the impingement axis and does not have fluctuations as doublet injector. More homogeneous and stable structure is observed in triplet jet injector analyses.

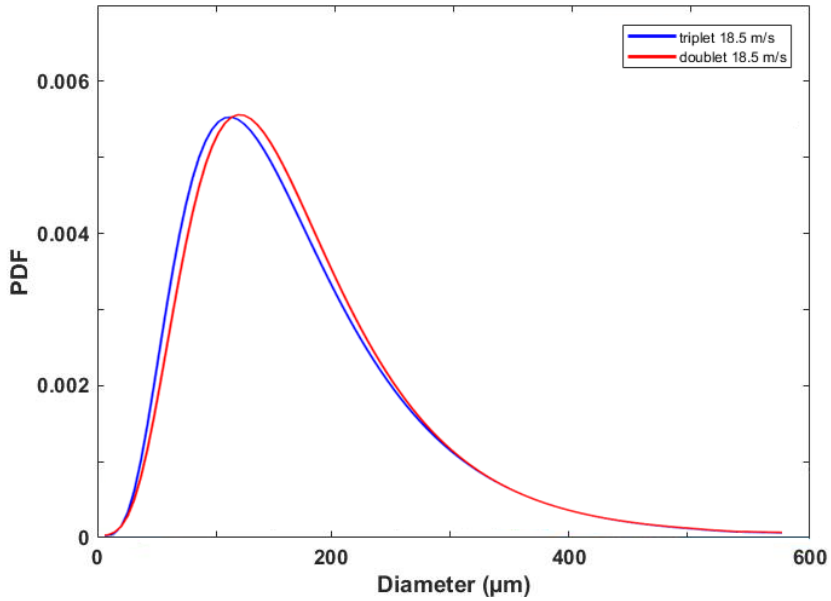

Figure 14. Log-normal droplet size distribution of doublet and triplet injectors

Triplet impingement jet injector analyses also performed for different inlet velocity values. In Figure 15, log-normal distributions of droplet size are given for different velocity values. It is clearly that, with increasing inlet velocity droplets are getting smaller. Peak value dropped to around 80 μm.

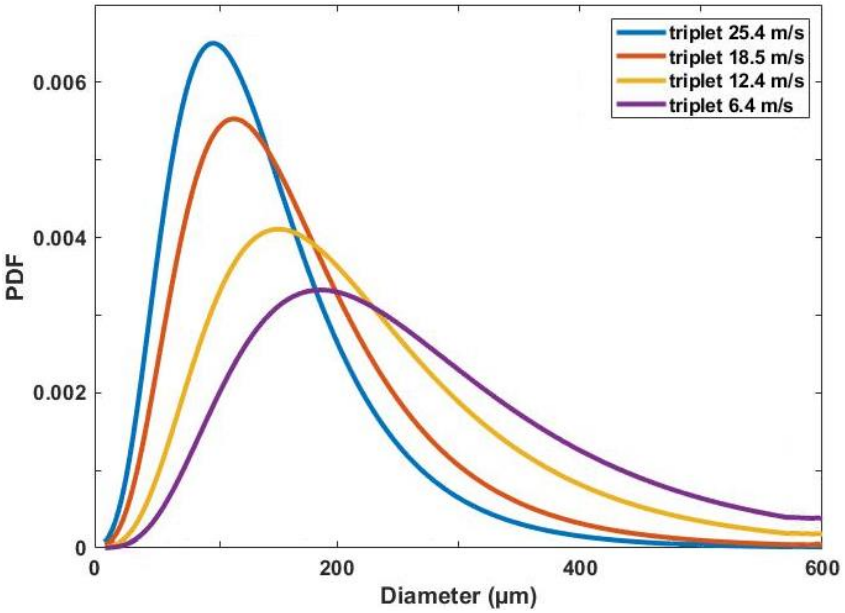

Figure 15. Log-normal droplet size distribution of triplet injector at different velocities

When the relative velocity between air and water increases, droplet size reduces and also sheet break-up length decreases but if the liquid sheet velocity increases, break-up length increases. In this study, the sheet velocity increased with third injector, so the liquid sheet began to disintegrate further away from the point of impingement. In this work, the velocity is more dominant on the droplet size distribution than the injector types. The effects of these two types of injectors on combustion efficiency can be examined for future studies. The liquid sheet of triplet injector is more homogeneous and more stable so it can affect the combustion efficiency in a good way. In addition, how the angle between the jets affects the droplet size distribution can be investigated.

References

Anderson, W. E., Ryan, H., Santoro, R., & Hewitt, R. (1995). Combustion Instability Mechanism in Liquid Rocket Engines Using Impinging Jet Injectors. 31st Joint Propulsion Conference and Exhibit. San Diego, CA, U.S.A: AIAA 95-2357.

Arienti, M., Li, X., Soteriou, M. C., Eckett, C. A., Sussman, M., & Jensen, R. J. (2013). Coupled Level-set/Volume-of-Fluid Method for the Simulation of Liquid Atomization in Propulsion Device Injectors. Journal of Propulsion and Power, 29, 147-157.

Inoue, C., Watanabe, T., & Himeno, T. (2008). Study on Atomization Process of Liquid Sheet Formed by Impinging Jets. 44th AIAA/ASME/SAE/ASEE Joint Propulsion Conference & Exhibit, Joint Propulsion Conferences. Hartford, CT: AIAA 2008-4847 (2008).

Lefebvre, A. H., & McDonell, V. G. (2017). Atomization and Sprays. CRC Press.

Ryan, H., Anderson, W., Pal, S., Santoro, & R.J. (1995). Atomization Characteristics of Impinging Liquid Jets. Journal of Propulsion and Power, 11, 135-145.

Siemens. (2019). Simcenter Star-CCM+ Theory Guide. Siemens PLM Software